

On self-preservation and log-similarity in a slightly heated axisymmetric mixing layer

F. Thiesset, V. Schaeffer, L. Djenidi,^{a)} and R. A. Antonia

School of Engineering, University of Newcastle, NSW 2308 Callaghan, Australia

(Received 4 May 2014; accepted 11 July 2014; published online 28 July 2014)

This paper reports an experimental investigation of self-preservation for one- and two-point statistics in a slightly heated axisymmetric mixing layer. Results indicate that the longitudinal velocity fluctuation u seems to approach self-preservation more rapidly than either the transverse velocity fluctuation v or the scalar fluctuation θ . The Reynolds number $Re_\delta = U_0\delta/\nu$ (U_0 being the jet inlet velocity and δ the momentum thickness) that ought to be achieved for the one-point statistics to behave in a self-similar fashion is assessed. Second, the relevance of different sets of similarity variables for normalizing the energy spectra and structure functions is explored. In particular, a new set of shear similarity variables, emphasizing the range of scales influenced by the mean velocity and temperature gradient, is derived and tested. Since the Reynolds number based on the Taylor microscale increases with respect to the streamwise distance, complete self-preservation cannot be satisfied; instead, the range of scales over which spectra and structure functions comply with self-preservation depends on the particular choice of similarity variables. A similarity analysis of the two-point transport equation, which features the large scale production term, is performed and confirms this. Log-similarity, which implicitly accounts for the variation of the Reynolds number, is also proposed and appears to provide a reasonable approximation to self-preservation, at least for u and θ . © 2014 AIP Publishing LLC. [<http://dx.doi.org/10.1063/1.4890994>]

I. INTRODUCTION

The hypothesis of self-preservation which assumes that the flow is governed by a single set of length, velocity, and scalar scales has been extensively applied for describing the spatio-temporal evolution of some canonical turbulent flows. Among the literature, this hypothesis has led to significant contributions to the study of homogeneous isotropic turbulence (Refs. 1–4 among others) and to scalar fluctuations evolving in isotropic turbulence (e.g., Refs. 5–9). Self-preservation has also been applied to homogeneous shear turbulence,^{10,11} wake flows,^{12–17} turbulent jets,^{13,18–22} and turbulent shear-layers.^{23–27} It is important to stress that the quest for self-preserving solutions has motivated many aspects of research in turbulence since it has the tremendous advantage of reducing partial differential equations to ordinary differential equations.

Generally speaking, one-point statistics (mean values, Reynolds stress, etc.) as well as two-point statistics (e.g., spectra or structure functions) can be studied under the constraints imposed by self-preservation. When applied to two-point statistics, complete self-preservation implicitly suggests that all scales behave similarly. It is now well known that this requires the Reynolds number R_λ based on the Taylor microscale λ (to be defined later) and a typical fluctuation u' to be constant (see, e.g., Refs. 2–4 and 21). Indeed, the constancy of R_λ ensures that the ratios between the different length-scales (the integral scale, the Taylor microscale, the Kolmogorov scale) and velocity scales (for instance, the rms, the Kolmogorov velocity, ...) are also constant.^{8,21,22} In such cases, *inner* scales (e.g., the Taylor microscale or the Kolmogorov length-scale) can be used interchangeably with *outer*

^{a)}Electronic mail: Lyazid.Djenidi@newcastle.edu.au

scales (the integral length-scale, for example) because they all behave similarly. This circumvents the question of which are the most relevant similarity variables to be used for normalization. The only flows for which this constraint is respected is the far field of the round jet (at least along the axis), the far field of a cylinder wake (preliminary results gathered by our group suggest that x/D , where D is the diameter of the cylinder, needs to exceed a value of about 200 before R_λ is constant), and the initial period of decay of grid turbulence at an infinitely large Reynolds number. Therefore, the range of flows complying with self-preservation appears to be very limited especially since the third flow is unlikely to be realizable.

For turbulent flows for which R_λ varies significantly, complete self-preservation, i.e., self-similarity of spectra or correlation functions at all scales, cannot be satisfied. Consequently, the range of scales satisfying self-preservation depends on the particular choice of similarity variables (see, e.g., Refs. 4, 8, and 9), and it appears that outer variables are relevant for normalizing the large-scales, while inner variables are likely to be appropriate at small-scales. Therefore, performing a self-similarity analysis in flows where R_λ varies significantly remains a challenging task.

On the other hand, log-similarity has been subsequently proposed as an alternative to the classical picture of self-similarity. Log-similarity was first applied to temperature spectra in Rayleigh-Bénard convection²⁸ and was shown to hold over an impressive range of Rayleigh numbers. Nelkin²⁹ soon suggested the applicability of such a similarity for fully developed homogeneous isotropic turbulence. The main theoretical arguments in favour of the plausibility of log-similarity rely on a multifractal analysis^{28,30,31} and variational approaches of small-scale intermittency.³¹ Clearly, the relevance of such approaches when the Reynolds number is only moderate remains somewhat debatable.

The main objective of the present study is to investigate in detail the accuracy with which self-similarity is satisfied in a heated axisymmetric shear layer. In particular, the focus is on the approach towards self-preservation for one-point statistics, velocity-temperature correlations as well as two-point statistics such as spectra and structure functions. Both dynamical and scalar fields are examined. While the validity of self-preservation in the axisymmetric shear layer does not need to be further demonstrated, it is of interest to extend the analysis to higher-order statistics (up to the third-order), previous studies being usually limited to first- and second-order statistics.²³⁻²⁷ Note that the axisymmetric shear layer has been less studied than the plane mixing layer for which extensive measurements of high-order statistics and small-scale quantities have been performed, for example, by Refs. 32 and 33. In addition, to the best of our knowledge, extending the study of self-preservation to two-point statistics in the shear layer has not been attempted previously. This seems quite surprising, given that the shear layer is an archetypal flow, which feels the presence of a strong shear as well as a persisting organized motion.²⁴ Consequently, this particular flow appears to be nicely tailored for studying the interactions between different ranges of scales and how they could reach a possible equilibrium. For example, it is of interest to assess the range of scales directly influenced by the mean shear and the mean temperature gradient, how they differ in behaviour with the small-scales and which quantities are relevant for normalizing them. Moreover, the Reynolds number R_λ is known to increase with respect to the streamwise distance. The shear layer is thus perfectly suited for investigating the departure from complete self-preservation associated with the spatial variation of R_λ . Further, the relevance of the log-similarity, whose major advantage is to implicitly account for this variation, can also be assessed.

This paper is organized as follows. The experimental apparatus is first outlined in Sec. II. Second, the approach towards self-similarity for one-point statistics is investigated in Sec. III. The analysis is further extended to two-point statistics in Sec. IV. For this purpose, four different sets of similarity variables are tested both analytically (Sec. IV B) and experimentally (Sec. IV C), notably the shear similarity variables which are defined in Sec. IV A. Log-similarity is then applied to the experimental data in Sec. IV D. Conclusions are finally drawn in Sec. V.

II. EXPERIMENTS

Experiments were performed in a mixing layer associated with a slightly heated round jet. The jet facility has been described in detail, for example, in Refs. 21 and 34. The jet nozzle has a diameter of $D = 55\text{mm}$, and the jet exit velocity U_0 was set to 12.3 m s^{-1} . The corresponding

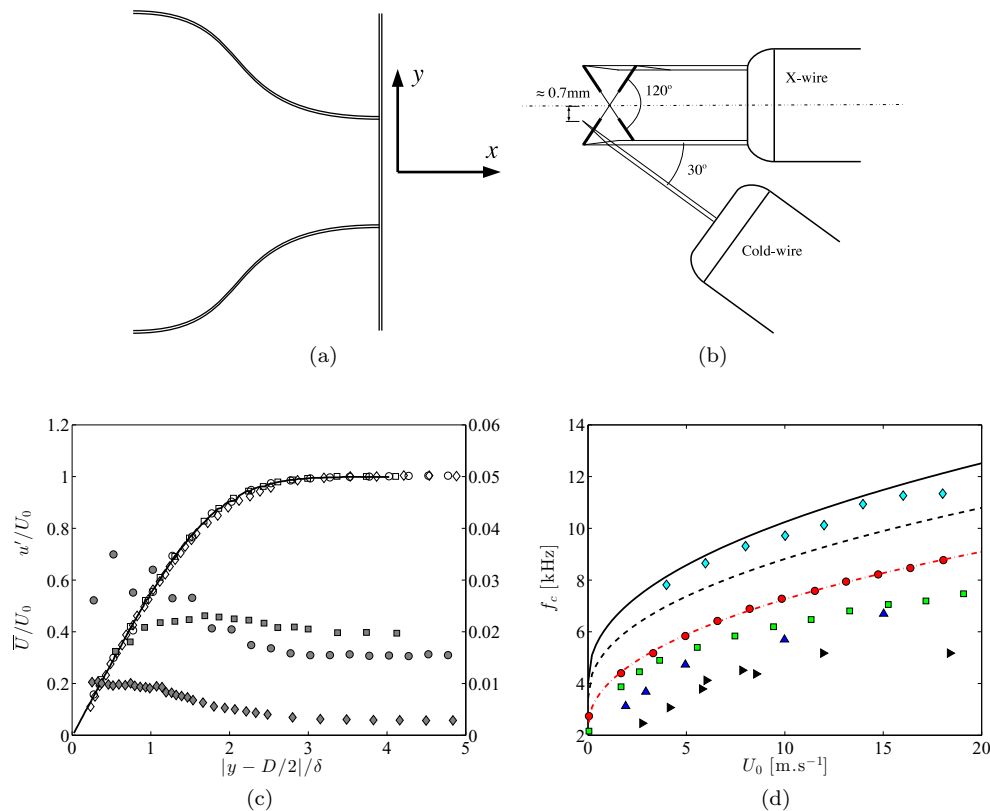


FIG. 1. (a) Sketch of the jet facility and coordinate system. (b) Schematic of the hot-cold wire probe used for the present measurements. (c) Mean velocity (open symbols) and rms profiles (closed symbols) near the jet exit. \circ present measurements, \square data from Burattini *et al.*,³⁴ \diamond data from Hussain and Clark,³⁵ — Blasius profile. (d) Cut-off frequency of the cold wire measured using a square wave current injection. \circ presents measurements with a Pt $0.6 \mu\text{m}$ wire probe, \square presents measurements with a Pt-10%Rh $0.63 \mu\text{m}$ wire probe, \diamond data from Lemay and Benaïssa⁴⁰ with a Pt-10%Rh $0.58 \mu\text{m}$ wire probe submitted to the current injection test, \triangle data from Fiedler⁴¹ using a Pt-10%Rh $0.63 \mu\text{m}$ wire probe and a chopped laser beam, \triangleright data from Antonia *et al.*⁴² using a Pt-10%Rh $0.63 \mu\text{m}$ wire probe and the pulsed wire technique. — and - - - correspond to the theoretical expectations for a Pt $0.6 \mu\text{m}$ and a Pt-10%Rh $0.63 \mu\text{m}$ wire, respectively, and — \cdot — is the fit using the functional $f_c = A_1 + A_2\sqrt{U_0} + A_3U_0$, with $A_1 = 2.06$, $A_2 = 1.70$, and $A_3 = -0.18$.

Reynolds number $Re_D = U_0D/\nu$ is 46 700 (ν is the kinematic viscosity). Some measurements were carried out in the boundary layer at the jet exit and it was found that the mean velocity was consistent with a Blasius profile (see Fig. 1(a)). The maximum turbulence level in the boundary layer was found to be of about 3.5%, i.e., in the range of typical experiments^{26,34,35} (see Fig. 1(c)). The air at the inlet of the centrifugal blower was heated using an electrical fan heater. The jet facility was also completely lagged with a glass wool layer covered with a metallic foil overlay to obtain a more uniform mean temperature profile at the exit. The homogeneity of the temperature profile at the jet exit was checked using a thermocouple and found to be within 10%. The temperature excess $\theta_0 \approx 15^\circ\text{C}$ on the jet centerline. The ratio Gr/Re_D^2 ($Gr = gD^3(\theta_0 + T_a)/\nu^2T_a$ is the Grashof number with T_a is the ambient absolute temperature and g is the gravity acceleration) was about 3.5×10^{-3} indicating that temperature can be considered as a passive scalar, since buoyancy is negligible. Simultaneous velocity and temperature measurements were performed at six different downstream distances from the jet nozzle $1.5 \leq x/D \leq 4$ and for several transverse positions traversing the shear layer.

The longitudinal U and transverse V velocity components in the x in y direction respectively (Fig. 1(a)) were measured using a X-wire probe, consisting a two Wollaston (Pt-10%Rh) wires of diameter $2.5 \mu\text{m}$ and typical length of 0.5 mm. The angle between the two wires was chosen to be about 60° in order to capture high velocity angles that may occur in this particular region of the flow

(see Fig. 1(b)). The lateral separation between the two wires were about 0.5 mm. The hot-wires were operated by in-house constant temperature anemometer at an overheat ratio of 1.5. The hot-wire voltages were corrected from temperature variations using³⁶

$$E_c(t) = E_m(t) \left(\frac{T_w - T_{cal}}{T_w - T(t)} \right)^{1/2}, \quad (1)$$

where E_c and E_m are the corrected and measured voltages, respectively. T_w , T_{cal} , and $T(t)$ are, respectively, the wire temperature, the air temperature during calibration, and the air temperature during measurements. Calibration was made *in situ* in the potential core of the jet. The look-up table method³⁷⁻³⁹ was employed for calibrating the X-wire probe with velocity magnitudes in the range 0–30 m s⁻¹ with velocity increments of 1 m s⁻¹ and angles in the range $\pm 60^\circ$ with increments of 10° .

A Wollaston (Pt) wire of nominal diameter $d_w = 0.6 \mu\text{m}$, operated by in-house constant current circuits, was used for temperature measurements. The current supplied to the wire was 0.1 mA, so that the wire was essentially insensitive to the flow velocity. The wire was etched for a length $l_w \approx 0.6$ mm, yielding a ratio l_w/d_w of about 1000. A square-wave injection technique^{34,40} was adopted for the determination of the frequency response of the cold wire. As emphasized in Fig. 1(d), the Pt-0.6 μm wire was chosen since the cut-off frequency f_c was found to be larger than for a Pt-10%Rh-0.63 μm wire. The instantaneous temperature signal is then corrected following the method of Ref. 43. The cut-off frequency was first fitted using the functional $f_c = 1/2\pi\tau_w = A_1 + A_2\sqrt{U_0} + A_3U_0$, which allows to compute the instantaneous time constant $\tau_w(t)$ knowing the instantaneous velocity magnitude $\sqrt{U^2(t) + V^2(t)}$. The corrected temperature θ is then calculated from measured temperature θ_m following $\theta = \theta_m + \tau_w(t)\partial\theta_m/\partial t$. The correction method of Ref. 40 was also tested and led to some very similar corrections for the temperature signal and related statistics. The cold-wire probe has an angle of 30° with the X-wire probe, the latter being aligned with the jet axis (Fig. 1(b)). The cold-wire is displaced by about 0.7 mm from the hot-wires in order to avoid interferences (Fig. 1(b)).

The output signals from anemometer channels, operating the cold and hot wires, were passed through buck-and-gain circuits and low-pass filtered at a frequency f_c slightly larger than the Kolmogorov frequency $f_K = \bar{U}/2\pi\eta_K$ (\bar{U} is the mean velocity and η_K is the Kolmogorov length-scale to be defined later). The signals were acquired using a National instrument 16 bits A/D converter at a sampling frequency $f_s = 2f_c$. Convergence of velocity and scalar statistics was checked and found to be satisfactory. The high turbulence level in the shear layer can significantly alter the reliability of the classical Taylor hypothesis $x \equiv \bar{U}t$. Therefore, for calculating two-point statistics, a local convection velocity is used in the Taylor hypothesis; for this purpose we followed the same procedure as outlined in Ref. 21.

III. SELF-PRESERVATION OF ONE-POINT STATISTICS

We first pay particular attention to the approach towards self-preservation for one-point statistics. At this stage, the relevant scales are the inlet velocity U_0 for the velocity field, the temperature excess $\theta_0 = T(y=0) - T_a$ for the temperature field, while the normalized transverse coordinate ξ is given by

$$\xi = -\frac{y - y_{0.5}}{\delta}. \quad (2)$$

$y_{0.5}$ is the position y where the longitudinal mean velocity \bar{U} is equal to $U_0/2$ (hereafter, the overbar denotes time averaged values) and the momentum thickness δ is defined by

$$\delta = \int_0^\infty \frac{\bar{U}(y)}{U_0} \left(1 - \frac{\bar{U}(y)}{U_0} \right) dy. \quad (3)$$

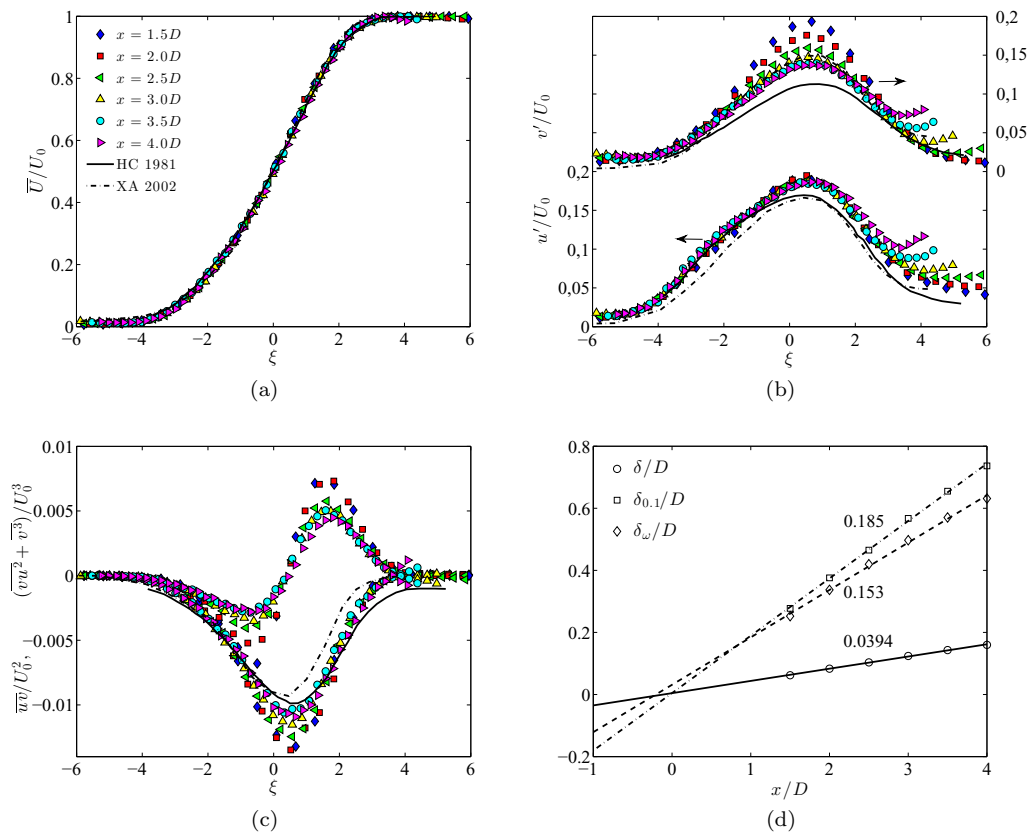


FIG. 2. Profiles of (a) mean velocities, (b) rms, (c) higher order statistics, as a function of the normalized transverse distance ξ for different downstream positions. $\diamond x = 1.5D$, $Re_\delta = 2.8 \times 10^3$. $\square x = 2D$, $Re_\delta = 3.7 \times 10^3$. $\triangleleft x = 2.5D$, $Re_\delta = 4.6 \times 10^3$. $\triangle x = 3D$, $Re_\delta = 5.5 \times 10^3$. $\circ x = 3.5D$, $Re_\delta = 6.4 \times 10^3$. $\triangleright x = 4D$, $Re_\delta = 7.2 \times 10^3$. — Hussain and Clark³⁵ and — · — Xu and Antonia.⁴⁴ (d) Streamwise evolution of the shear layer length-scales δ , $\delta_{0.1}$, and δ_ω together with their respective linear fit (lines).

Here δ can be used interchangeably with the shear-layer thickness $\delta_{0.1} = y_{0.9} - y_{0.1}$ ($y_{0.9}$ and $y_{0.1}$ are the transverse locations where \bar{U}/U_0 is 0.1 and 0.9, respectively) and the vorticity thickness δ_ω ,

$$\delta_\omega = \frac{U_0}{\max\left(\frac{\partial \bar{U}}{\partial y}\right)} \quad (4)$$

since δ , $\delta_{0.1}$, and δ_ω all behave similarly with the downstream distance x . More precisely, all these length-scales are known to be proportional to x (e.g., Refs. 24, 26, and 35).

Figs. 2(a)–2(c) present the first-, second-, and third-order statistics of the velocity field normalized by the relevant quantities. A compilation of some published experimental data are also given to assess the accuracy of the present measurements. While the agreement between the present measurements and the published data of Refs. 35 and 44 is satisfactory for the mean velocity \bar{U}/U_0 , there are some slight differences as far as second-order statistics are concerned. These discrepancies may be first attributed to some differences in the initial conditions,^{26,27,44} especially the turbulence level which is slightly larger than that of Ref. 35. Second, and perhaps to a larger extent, these departures may be due to the particular probe used for measuring u and v (a 60° X-wire probe being likely to be more adequate than a 45° in this region of the flow) and to the calibration method (the look-up table being more reliable than the yaw-angle method especially in highly turbulent flows³⁹).

It is observed that the longitudinal velocity component reaches a self-similar state rather quickly and there is a perfect collapse of both \bar{U}/U_0 and u'/U_0 (the prime stands for the rms value) for all the range of measurements $1.5D \leq x \leq 4D$ (only the range of $\xi \leq 3$ is considered for analysing self-similarity since for higher transverse distances, fluctuations in the potential core of the jet

progressively increase). However, the collapse for the transverse velocity component v is attained less rapidly, and a distance of $x = 3.5D$ ($\equiv Re_\delta = U_0\delta/\nu = 6.4 \times 10^3$) has to be reached for v'/U_0 to behave in a self-similar fashion. This remark holds also for the Reynolds stress \overline{uv}/U_0^2 and higher-order statistics such as the kinetic energy flux $(\overline{vu^2} + \overline{v^3})/U_0^3$. Note that some measurements at a larger distance from the jet nozzle would have been necessary to confirm this since the assessment of self-similarity relies only on the two profiles at $x = 3.5D$ and $4D$. However, the present measurements seem to indicate that a Reynolds number $Re_\delta = 6.4 \times 10^3$ has to be attained for self-preservation to be satisfied for all velocity components. In Ref. 35, it was observed that v'/U_0 was self-similar beyond $x = 0.71D$ (no measurements were made at smaller distances) corresponding to $Re_\delta \approx 10^4$ which is consistent with our observation. Noticeable is the fact that the maximum value for both v'/U_0 and \overline{uv}/U_0^2 progressively decreases before reaching its self-similar value of about 0.14 and -0.01 , respectively. This may be associated with the presence of coherent structures, known as the Kelvin-Helmholtz vortices,²⁴ whose energetic contribution to v' and \overline{uv} decreases as x increases. This point will be further confirmed when analysing two-point statistics.

The downstream evolution of the shear layer characteristic length-scales δ , $\delta_{0,1}$, and δ_ω is plotted in Fig. 2(d), together with their respective linear fit. The proportionality between δ , $\delta_{0,1}$, and δ_ω and the streamwise distance x is well verified for the present measurements. The slope for $\partial\delta/\partial x$ is equal to 0.0394 which is slightly larger than the commonly encountered values generally in the range [0.029–0.037].^{26,27} $\partial\delta_{0,1}/\partial x = 0.185$ which is comparable with some published values [0.17–0.23] (Ref. 26 and references therein). $\partial\delta_\omega/\partial x = 0.153$ in agreement with the data of Brown and Roshko²⁴ [0.145–0.22]. The linearity of δ , $\delta_{0,1}$, and δ_ω with x confirms that they can be used interchangeably for normalizing the transverse distance y .

We now turn our attention to the scalar field. For convenience, the temperature excess θ relative to the ambient temperature T_a is considered here, viz., $\theta = T - T_a$. Experimental data for the mean scalar value $\bar{\theta}$, and the rms of scalar fluctuations θ' , the velocity-temperature correlations $\overline{u\theta}$, $\overline{v\theta}$ and the temperature flux $\overline{v\theta^2}$, normalized by the appropriate set of similarity variables (the temperature excess $\Delta\theta_0 = T(y=0) - T_a$ and the momentum thickness δ), are given in Figs. 3(a), 3(b), 3(c), and 3(d), respectively. Even though comparing the plane and axisymmetric shear layer may be rather misleading, the mean temperature profile we obtain is roughly consistent with that inferred from Ref. 45. The mean and fluctuating temperature fields (Figs. 3(a) and 3(b)) appear to reach a self-similar state around $x = 3.5D$, i.e., at the same position as the transverse velocity component. The velocity-temperature correlations $\overline{u\theta}$ and $\overline{v\theta}$ (Fig. 3(c)) appear to be of opposite sign and also attain self-preservation at a streamwise distance of $x = 3.5D$. The transverse temperature flux, i.e., the transport of temperature fluctuations θ^2 by the transverse velocity component v is represented in Fig. 3(d). Here again, the profiles are roughly consistent with self-similarity for downstream distance $x \geq 3.5D$.

In summary, one-point statistics of the velocity components u , v and the scalar field θ reach a self-preserving state following different approaches. It is observed that statistics of u attain self-similarity more rapidly than that of v and θ . Arguably, this difference in behaviour is likely to be attributed to the contribution of the coherent motion which is mostly visible on v and diminishes with the streamwise distance. This statement can be further confirmed using energy spectra and structure functions on which we now turn our attention.

IV. SELF-PRESERVATION OF TWO-POINT STATISTICS

Extending the analysis of self-preservation to two-point statistics provides a deeper insight into the flow details since the evolution of the turbulence structure at a given scale can be assessed. In the present study, the relevance of four different sets of similarity variables for normalizing energy spectra and structure functions is tested

- The Kolmogorov variables⁴⁶ $u_K = (\nu\bar{\epsilon})^{1/4}$ and $\eta_K = (\nu^3/\bar{\epsilon})^{1/4}$ ($\bar{\epsilon} = 15\nu\overline{(\partial u/\partial x)^2}$ is the mean kinetic energy dissipation rate) for normalizing the velocity spectra and structure functions. For the temperature field, the Batchelor variables are used $\theta_B = \sqrt{\bar{\epsilon}_\theta\eta_K/u_K}$ and $\eta_B = \eta_K/Pr$ (the

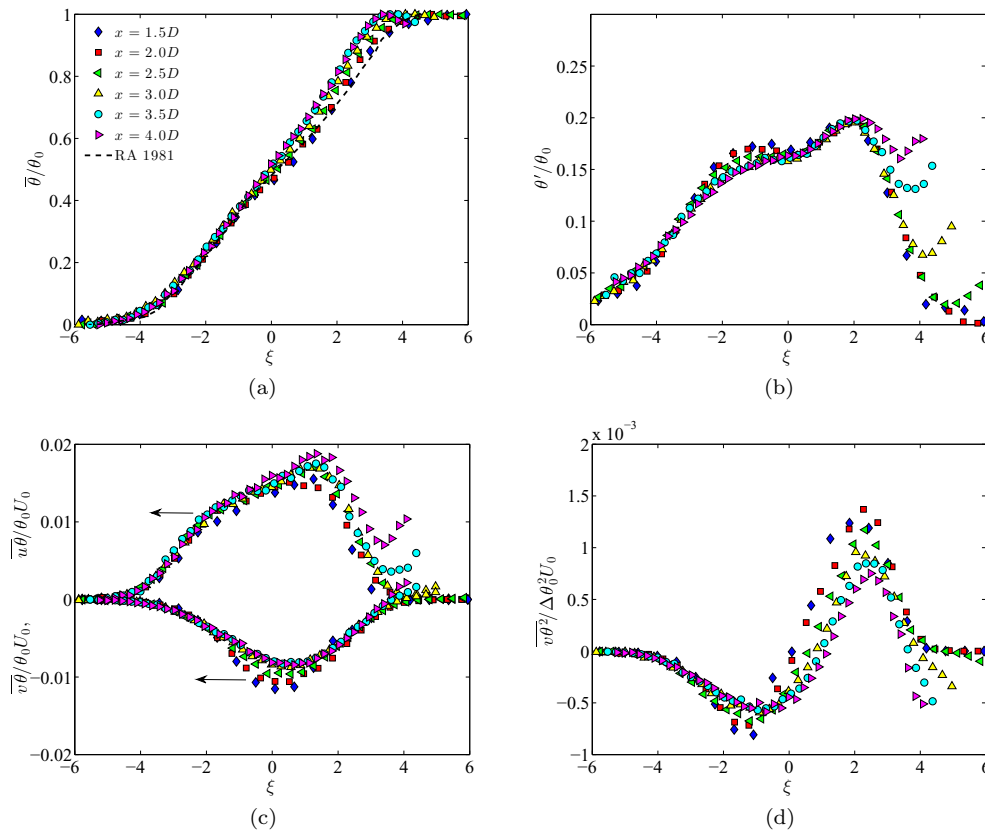


FIG. 3. Profiles of (a) mean scalar values, (b) rms of scalar fluctuations, (c) and (d) velocity-scalar correlations as a function of the normalized transverse distance ξ for different downstream positions. See Fig. 2(a) for legend. In (a) ---- corresponds to the data of Rajagopalan and Antonia⁴⁵ obtained in the shear layer of a heated plane jet.

Prandtl number $Pr = \nu/\kappa$ with κ the temperature diffusion coefficient and $\bar{\epsilon}_\theta = 3\kappa(\overline{\partial\theta/\partial x})^2$ is the scalar dissipation rate).

- The George similarity variables,² i.e., the velocity variance $\overline{u_\alpha^2}$ (u_α stands for either u or v) and the Taylor microscale $\lambda = \sqrt{15\nu\overline{u^2}/\bar{\epsilon}}$ for the velocity field and the temperature variance $\overline{\theta^2}$ and the Corrsin microscale $\lambda_\theta = \sqrt{3\kappa\overline{\theta^2}/\bar{\epsilon}_\theta}$ for the scalar field.
- The outer variables. The term “outer variables” should be understood as macroscopic scales, for instance, δ is the characteristic length-scale and U_0 and θ_0 are used for normalizing the dynamical and scalar field, respectively.
- The shear variables which are defined below.

A. Definition and assessment of the shear characteristic scales

In order to derive the shear characteristic scales, we will consider the simplified case of homogeneous shear turbulence. It is important to stress that this hypothesis might not be strictly applicable to the axisymmetric shear layer since, e.g., the turbulent diffusion term is likely to contribute³² to the energy budget. However, it is obvious that the production mechanism associated with the mean shear is a predominant feature of the shear layer, especially at a transverse position $\xi = 0$ (see Ref. 32).

Let us first recall the arguments of Ref. 47 that allow to derive the shear length-scale for the dynamical field. In a turbulent flow dominated by the mean shear, the scale-by-scale budget is given

by¹¹

$$6\nu \frac{\partial(\overline{\Delta u})^2}{\partial r} - \overline{(\Delta u)^3} - \frac{6}{r^4} \int_0^r s^4 \overline{\Delta u \Delta v} S_u ds = \frac{4}{5} \bar{\epsilon} r. \quad (5)$$

Here $\Delta\beta = \beta(x+r) - \beta(x)$ is the velocity increment of the quantity $\beta \equiv u, v, \theta$ between two points separated by a distance r . The first term on LHS of Eq. (5) corresponds to the viscous term and dominates at rather small scales. The second term is identified as the nonlinear transfer term whose contribution is mostly perceptible at intermediate scales. The third term corresponds to a production term through the mean velocity gradient $S_u = \partial\bar{U}/\partial y$ and dominates at rather large scales.^{11,47} Casciola *et al.*⁴⁷ suggested that the shear length-scale L_S^u first defined on dimensional arguments by Corrsin⁴⁸ can be identified as the scale for which the production term in Eq. (5) balances the nonlinear transfer term, i.e.,

$$L_S^u \equiv r \text{ such as } \overline{(\Delta u)^3}(r) = \frac{6}{r^4} \int_0^r s^4 \overline{\Delta u \Delta v} S_u ds. \quad (6)$$

Assuming $\overline{(\Delta u)^3} \propto \bar{\epsilon} r$ and $\overline{\Delta u \Delta v} \propto (\bar{\epsilon} r)^{2/3}$ (which strictly hold only at very high Reynolds numbers), one obtains

$$L_S^u = \sqrt{\frac{\bar{\epsilon}}{S_u^3}}. \quad (7)$$

Then, from the one-point energy budget which features only the production and dissipation terms, one can write

$$U_S^2 S_u \sim \bar{\epsilon}, \quad (8)$$

which leads to a shear characteristic velocity $U_S = \sqrt{\bar{\epsilon}/S_u}$. A similar analysis can be carried out for the scalar field by first recalling the scale-by-scale budget of $\overline{(\Delta\theta)^2}$ in presence a mean temperature gradient⁴⁹

$$2\kappa \frac{\partial(\overline{\Delta\theta})^2}{\partial r} - \overline{\Delta u (\Delta\theta)^2} - \frac{2}{r^2} \int_0^r s^2 \overline{\Delta v \Delta\theta} S_\theta ds = \frac{4}{3} \bar{\epsilon}_\theta r, \quad (9)$$

where $S_\theta = \partial\bar{\theta}/\partial y$ is the mean temperature gradient. Assuming $\overline{\Delta u (\Delta\theta)^2} \propto \bar{\epsilon}_\theta r$ and $\overline{\Delta v \Delta\theta} \propto (\bar{\epsilon}_\theta r)^{1/3} (\bar{\epsilon}_\theta r)^{1/3} (\bar{\epsilon}_\theta/\bar{\epsilon})^{1/6}$, and identifying the scale L_S^θ for which the transfer term is equal to the production term, a shear length-scale for the scalar field can be similarly derived, viz.,

$$L_S^\theta = \sqrt{\frac{\bar{\epsilon}_\theta^{3/2}}{\bar{\epsilon}^{1/2} S_\theta^3}}. \quad (10)$$

One can further write the one-point budget of the temperature variance in the following form:

$$U_S \theta_S S_\theta \sim \bar{\epsilon}_\theta \quad (11)$$

yields a shear characteristic temperature $\theta_S = \bar{\epsilon}_\theta / S_\theta \sqrt{S_u/\bar{\epsilon}}$. L_S^u and L_S^θ allow to assess the range of scales which are in essence influenced by the presence of the mean shear and temperature gradient.⁴⁷ For $r \geq L_S^u$, L_S^θ , statistics of the velocity and scalar fields are dominated by production effects. On the other hand, the nonlinearity of the cascade mechanism is supposed to be sufficiently strong for scales smaller than L_S^β to behave in a universal manner, independently of the large scales.

The shear characteristics scales are plotted in Figs. 4(a) and 4(b). We plot the ratios δ/L_S^u and δ/L_S^θ since L_S^u and L_S^θ tend to infinity when the mean velocity and temperature gradient goes to zero. For $-4 \leq \xi \leq 2$, both L_S^u and L_S^θ are proportional to δ (see Fig. 4(a)), indicating that the shear length-scales are characteristic of rather large scale phenomena and fall into our definition of outer length-scales. The proportionality of L_S^u and L_S^θ to δ is simply related to the fact that $\bar{\epsilon} U_0^3/\delta$ and $\bar{\epsilon}_\theta U_0 \theta_0^2/\delta$ behave in a self-similar fashion. The ratios δ/L_S^u and δ/L_S^θ are about 3 at $\xi = 0$. It thus appears that L_S^u and L_S^θ are slightly smaller than the shear layer momentum thickness δ . The characteristic velocity U_S and temperature θ_S are also presented in Fig. 4(b). Here again, all curves

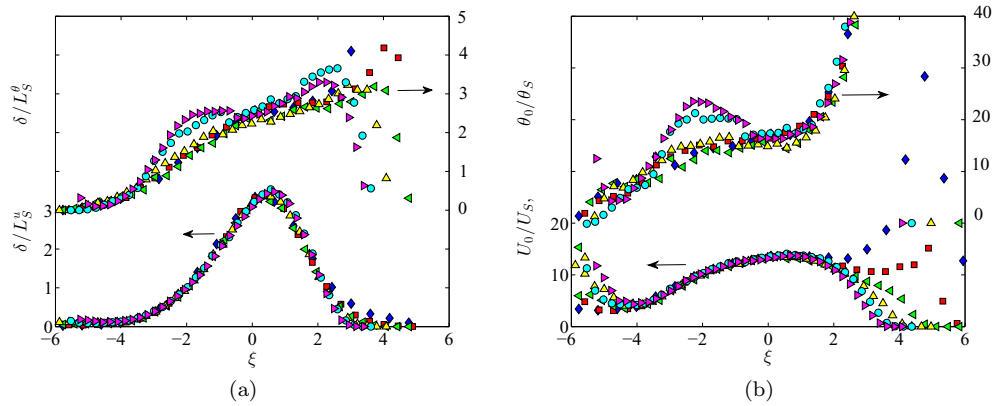


FIG. 4. (a) Profiles of δ/L_S^u and δ/L_S^θ , with the shear length-scales $L_S^u \equiv \sqrt{\bar{\epsilon}/S_u^3}$ and $L_S^\theta \equiv \sqrt{\bar{\epsilon}_\theta^{3/2}/\bar{\epsilon}^{1/2}S_\theta^3}$. (b) Profiles of U_0/U_S and Θ_0/Θ_S with the shear characteristic velocity $U_S = \sqrt{\bar{\epsilon}/S_u}$ and characteristic temperature $\theta_S = \bar{\epsilon}_\theta/S_\theta\sqrt{S_u/\bar{\epsilon}}$. See Fig. 2(a) for legend.

collapse reasonably well when normalized by U_0 and θ_0 , confirming that the shear characteristic scales can be identified as outer macro-scales.

B. *A priori* analysis of self-similarity for two-point statistics

The aim of this section is to analyse *a priori* the adequacy of the different similarity variables for normalizing two-point statistics. For this purpose, let us write second- and third-order structure functions in dimensionless form

$$\overline{(\Delta u)^2} = \mathcal{U}^2(x)f(r/\mathcal{L}), \quad (12a)$$

$$\overline{(\Delta u)^3} = \mathcal{U}^3(x)g(r/\mathcal{L}), \quad (12b)$$

$$\overline{(\Delta u \Delta v)} = \mathcal{U}^2(x)h(r/\mathcal{L}). \quad (12c)$$

Injecting Eqs. (12) into Eq. (5), yields

$$[2] \frac{f'}{\tilde{r}} + [F_1] \frac{g}{\tilde{r}} + [F_2] \frac{1}{\tilde{r}^5} \Gamma = [F_3], \quad (13)$$

where $\tilde{r} = r/\mathcal{L}$, the prime denotes differentiation with respect to \tilde{r} and $\Gamma = \int_0^{\tilde{r}} \tilde{s}^4 h d\tilde{s}$. The three functions appearing in Eq. (13) can be expressed as

$$F_1 = Re_{\mathcal{L}} = \frac{\mathcal{U}\mathcal{L}}{\nu}, \quad (14a)$$

$$F_2 = Re_{\mathcal{L}} \frac{S_u \mathcal{L}}{\mathcal{U}}, \quad (14b)$$

$$F_3 = \frac{4\bar{\epsilon}\mathcal{L}^2}{5\nu\mathcal{U}^2}. \quad (14c)$$

Complete self-similarity implies that all terms within brackets must behave similarly with x . Since one of them appears to be constant, then F_1 , F_2 , and F_3 should be also constant. Performing a similarity analysis without presupposing any particular form for \mathcal{U} and \mathcal{L} inescapably leads to several possible solutions depending on the constants F_1 to F_3 used for deriving them. For example, using Eqs. (14a) and (14c) leads to the Kolmogorov scales as the relevant length-scales, while the shear variables emerge from the use of Eqs. (14a) and (14b). However, none of them are suitable in terms of simultaneously satisfying all three constraints. This indicates that complete self-similarity cannot

be satisfied in the shear layer. To further describe this, let us assess the range of scales satisfying self-similarity depending on the particular set of similarity variables that is chosen.

- The Kolmogorov scales η_K and u_K . Recalling that in the shear layer $\bar{\epsilon} \propto x^{-1}$, we obtain

$$F_1 = \frac{u_K \eta_K}{\nu} \propto x^0, \quad (15a)$$

$$F_2 = \frac{S_u \eta_K}{u_K} \propto x^{-1/2}, \quad (15b)$$

$$F_3 = \frac{4 \bar{\epsilon} \eta_K^2}{5 \nu u_K^2} \propto x^0. \quad (15c)$$

Therefore, Kolmogorov similarity will be satisfied only at small scales for which the production term can be neglected. Arguably, this could be respected for scales in the range $0 \leq r \lesssim L_S^u$.

- George similarity variables $\lambda \propto x^{1/2}$ and $u' \propto x^0$,

$$F_1 = \frac{u' \lambda}{\nu} = R_\lambda \propto x^{1/2}, \quad (16a)$$

$$F_2 = R_\lambda \frac{S_u \lambda}{u'} \propto x^0, \quad (16b)$$

$$F_3 = \frac{4 \bar{\epsilon} \lambda^2}{5 \nu u'^2} \propto x^0, \quad (16c)$$

which indicates that George similarity is expected to be relevant for both very small and very large scales. However, some substantial departures from self-similarity are expected in the intermediate range where g is predominant.

- Outer similarity variables $\delta \propto x$ and U_0 ,

$$F_1 = \frac{U_0 \delta}{\nu} \propto x^1, \quad (17a)$$

$$F_2 = \frac{U_0 \delta S_u \lambda}{\nu u'} \propto x^1, \quad (17b)$$

$$F_3 = \frac{4 \bar{\epsilon} \delta^2}{5 \nu U_0^2} \propto x^1. \quad (17c)$$

The use of outer similarity variable will be relevant for the range of scales over which the viscous term $2f'/\tilde{r}$ is negligible. This is expected to be respected for scales in the range $r_c \lesssim r \leq \infty$, where r_c is the cross-over length-scale between the viscous and inertial range, viz., $r_c/\eta_K \approx 30^{3/4}$ (see, e.g., Ref. 4).

- Shear variables. Since $L_s^\theta \propto \delta$ and $U_s \propto U_0$, similar deductions can be drawn for the shear similarity variables.

An analogous analysis for Eq. (9), which is not reported here for the sake of clarity, leads to exactly the same conclusions. In summary, depending on the particular choice of similarity variables, the range of scales which satisfies self-preservation differs. The Kolmogorov variables are expected to be relevant for small and intermediate scales, departure from self-similarity when using George variables are likely to be observed at intermediate scales, while outer and shear characteristic scales are adequate for large and intermediate scales.

C. Similarity of energy spectra and structure functions

We first consider the degree with which energy spectra comply with self-similarity when normalized by the four different sets of similarity variables presented in Sec. IV B. In Figs. 5(a)–5(d) are plotted energy spectra at $\xi \approx 0$ in the range $1.5D \leq x \leq 4D$. In Fig. 5(a), a comparison of present spectra with those of Ref. 33 at $R_\lambda = 330$ is given. The agreement at intermediate and

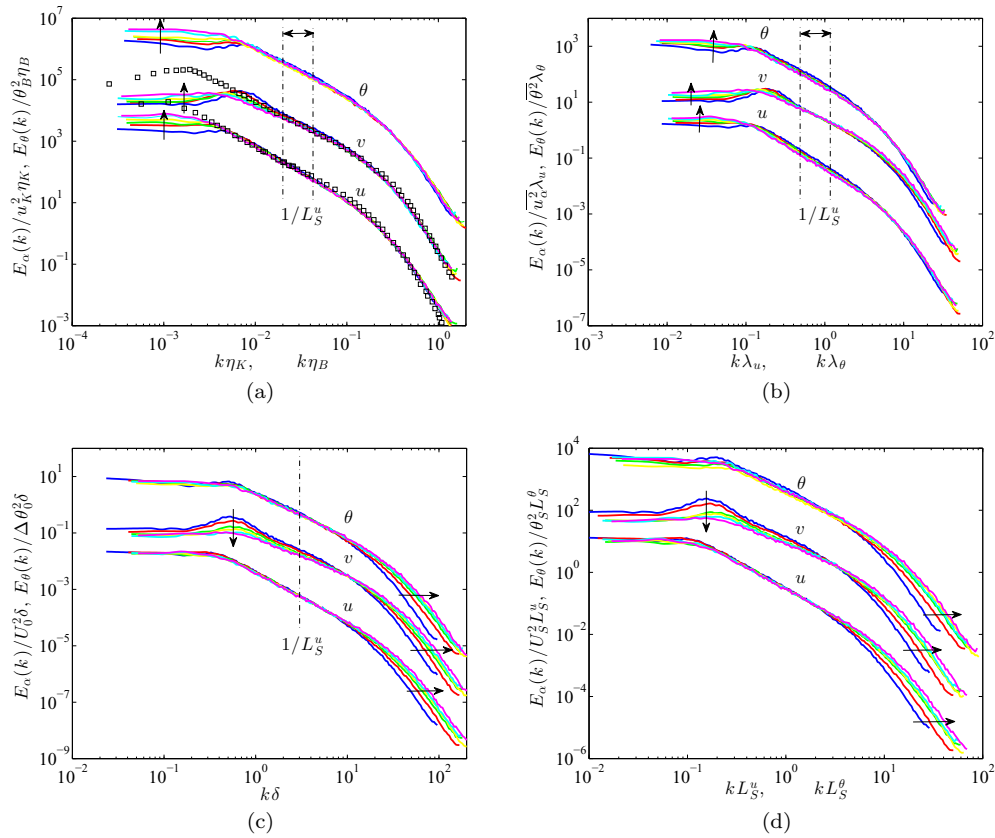


FIG. 5. Spectra in the range $1.5D \leq x/D \leq 4D$, normalized by (a) either Kolmogorov (u_K, η_K) or Batchelor scales (θ_B, η_B), (b) George similarity variables (u_a^2, λ), (θ^2, λ_θ), (c) outer variables δ and either U_0 or θ_0 , (d) shear length-scales (L_S^u, U_S) or (L_S^θ, θ_S). Spectra of v and θ are shifted upwards by a factor of 25 and 25^2 , respectively. The arrows indicate the direction of increasing x . In (a) square symbols correspond to the spectra measured by Ref. 33 in the plane shear layer.

small scales is almost perfect over two decades thus validating the present assessment of the energy spectra.

When velocity and temperature spectra are normalized by Kolmogorov and Batchelor scales, respectively, (Fig. 5(a)), one observes a perfect collapse for the dissipative scales up to the inertial range (strictly the restricted scaling range notwithstanding the quite low Reynolds number of the flow). Altogether, self-similarity is satisfied for wavenumbers $k\eta_{K,B} \geq 2 \times 10^{-2}$. For wavenumbers $k\eta_{K,B} < 10^{-2}$, there is a systematic increase in the amplitude of the spectra with x . This is explained by the non-constancy of the Reynolds number based on the Taylor microscale $R_\lambda = u'\lambda/\nu$ which increases from about 210 to 300 for $1.5 \leq x/D \leq 4$ (see, e.g., Refs. 4, 8, and 9). Note also that the range of wavenumbers over which spectra of u and θ satisfy self-similarity is wider than that of v . A peak in the v spectra is easily discernible around $k\eta_K \sim 10^{-2}$, which progressively diminishes in amplitude as x increases. At $x = 3.5D$, the spectrum of v follows closely that at $x = 4.0D$. The peak in the v spectrum is a footprint of the organized motion which monotonically shrinks as x increases. The peak ceases to be discernible for $x \geq 3.5D$. Arguably, the delay in the approach towards self-preservation for v that was observed for one-point statistics is likely to be due to these coherent structures and more particularly to the time they need before reaching a quasi-equilibrium state.

When using the George similarity variables² (see Fig. 5(b)), the collapse is satisfactory notwithstanding the slightly larger scatter in the inertial range. For v , a significant departure is also observed in the dissipative range. This differs from what is generally observed for example in grid^{4,8,9} or wake turbulence.¹⁷ In these flows, it is generally observed that the George similarity² is satisfied over a wider range of scales than with the Kolmogorov similarity. Here again, this feature is simply related

to the Reynolds number R_λ which substantially increases (by a factor 1.5) between $x = 1.5D$ and $x = 4D$.

Spectra normalized by the outer similarity variables δ , U_0 , and θ_0 are presented in Fig. 5(c). In contrast to the Kolmogorov or George similarity variables, the outer scales lead to a satisfactory collapse for the large-scales, including also a part of the pseudo-inertial range. However, there is a significant drift towards high wavenumbers as x increases. In addition to the similarity analysis as provided in Sec. IV B, this feature can be further explained by first recalling the definition of the normalized dissipation rate C_ϵ ,

$$\bar{\epsilon} = C_\epsilon \frac{U_0^3}{\delta} = \frac{C_\epsilon u^3}{A_I^3 \delta}. \quad (18)$$

$A_I = u'/U_0$ and C_ϵ were verified to be constant with x (see Figs. 2(b) and 4(a) for A_I and C_ϵ , respectively). Using Eq. (18), it can be shown that

$$\frac{\delta}{\lambda} = \frac{C_\epsilon}{15A_I^3} R_\lambda, \quad (19a)$$

$$\frac{\delta}{\eta_K} = \frac{C_\epsilon}{A_I^3} 15^{-3/4} R_\lambda^{3/2}, \quad (19b)$$

$$\frac{U_0^2}{u_K^2} = \frac{1}{A_I^2 \sqrt{15}} R_\lambda. \quad (19c)$$

Therefore, since R_λ increases, then the ratios δ/λ and δ/η_K increase and hence the normalized spectra progressively drift towards high wavenumbers. Unsurprisingly, similar deductions can be made when the shear length-scales are used for normalization (Fig. 5(d)) since L_S^u and L_S^θ are both proportional to δ .

We now turn our attention to the accuracy of the self-preservation hypothesis for second-order structure functions $\overline{(\Delta\beta)^2}$ ($\beta \equiv u, v, \theta$). While spectra and structure functions are simply related by

$$E_\beta(k) = \frac{\overline{\beta^2}}{\pi} \int_0^\infty \left(1 - \frac{\overline{(\Delta\beta)^2}}{2\beta^2}\right) \cos(kr) dr, \quad (20)$$

their physical interpretation differs. Indeed, spectra strictly represent the energy density at a given wavenumber, whereas structure functions are more likely to represent a cumulative energy distribution for scales $\leq r$ (e.g., Refs. 50–52). Second, $E_\beta(k) = [\text{m}^3 \text{s}^{-2}]$, whereas $\overline{(\Delta\beta)^2} = [\text{m}^2 \text{s}^{-2}]$ which means that, in addition to a velocity scale, a length scale has to be invoked for normalizing the spectra which is not the case for structure functions. Therefore, it is of interest to further study the accuracy with which self-preservation is satisfied in physical space.

Second-order structure functions normalized by the four different sets of similarity variables are plotted in Figs. 6(a)–6(d). Also included in Fig. 6(a) are the DNS structure functions of u and θ (Refs. 53, 54) for a plane mixing layer at a similar Reynolds number ($R_\lambda = 250$). In the intermediate range of scales, some very slight differences are discernible, which may be attributed to the differences in the initial/boundary conditions. However, the degree of agreement (especially in the dissipative range) is sufficiently satisfactory to unambiguously support the reliability of the present measurements. With Kolmogorov or Batchelor scales (Fig. 6(a)), one observes a perfect collapse for $\overline{(\Delta\beta)^2}$ at rather small scales, i.e., from the dissipative range up to the middle of the pseudo-inertial range. This is absolutely consistent with our theoretical expectations performed in Sec. IV B. Here again, the range of r over which $\overline{(\Delta u)^2}$ and $\overline{(\Delta\theta)^2}$ satisfy self-preservation is wider than for $\overline{(\Delta v)^2}$. A hint of a bump is discernible in the structure function of v for scales $r \approx 3 \times 10^2$, highlighting the persisting influence of the coherent motion.^{17,55,56} With the George variables (Fig. 6(b)), in agreement with section Sec. IV B, scatter is observed in the inertial range, especially for u and θ . As far as the transverse velocity component v is concerned, the departure from self-similarity surprisingly appears in dissipative range. This is most likely due to a bias when dividing $\overline{(\Delta v)^2}$ by v^2 , the latter being altered by the energy contribution of the coherent motion. As

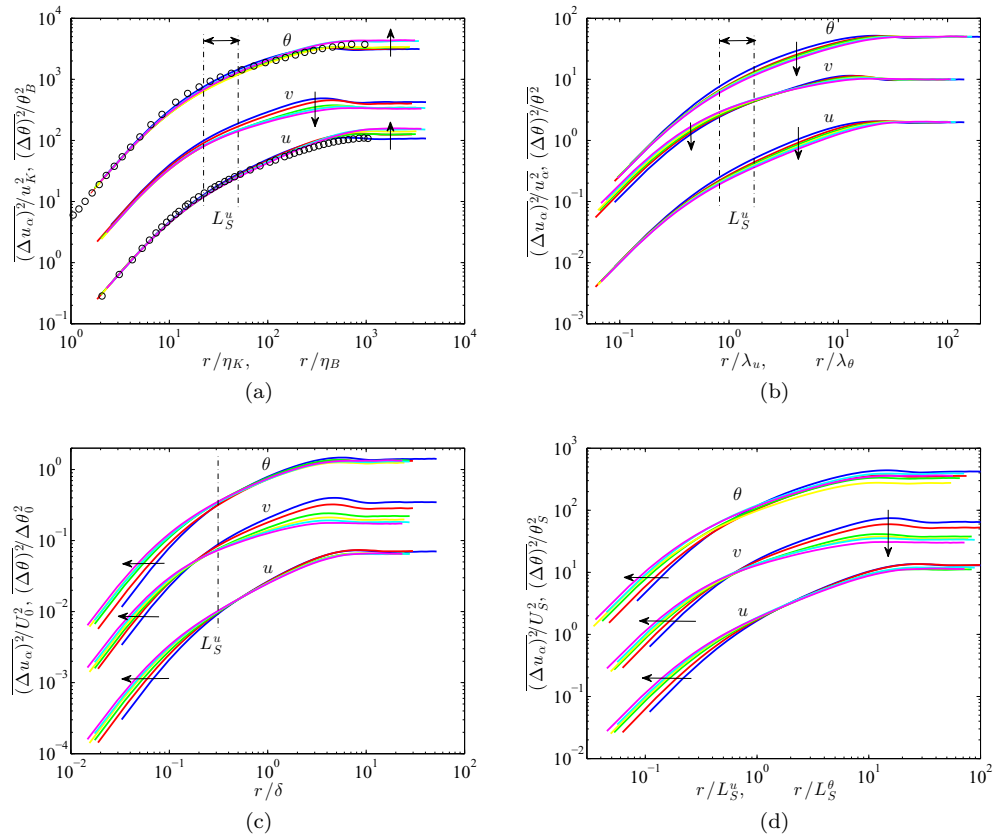


FIG. 6. Second-order structure functions in the range $1.5D \leq x/D \leq 4D$, normalized by (a) either Kolmogorov (u_K, η_K) or Batchelor scales (θ_B, η_B), (b) George similarity variables (u_s^2, λ), (θ^2, λ_θ), (c) outer variables δ and either U_0 or θ_0 , (d) shear length-scales (L_S^u, U_S) or (L_S^θ, θ_S). Structure function of v and θ are shifted upwards by a factor of 5 and 25, respectively. The arrows indicate the direction of increasing x . In (a), the symbols correspond to the data of Refs. 53 and 54.

was observed in the energy spectra, the use of either outer-variable (Fig. 6(c)) or shear-variables (Fig. 6(d)) leads to a reasonable collapse from large down to intermediate scales, whereas in the dissipative range, the different curves tend to drift towards small-scales when x increases.

In summary, complete self-preservation, i.e., self-similarity of energy spectra and structure functions over the whole range of scales or wavenumbers, appears to be untenable since R_λ significantly increases with respect to the streamwise distance. As a consequence, the range of scales over which self-similarity is observed depends on the particular choice of similarity variables. Kolmogorov variables are suitable for small up to intermediate scales. A significant departure from self-similarity is observed in the inertial range when using George similarity, whereas outer and shear variables are equally suitable for normalizing large and intermediate scales. These observations are in perfect agreement with the theoretical analysis presented in Sec. IV B.

The fact that large and small-scales both satisfy self-similarity with an overlap at intermediate scales, if normalized by their respective relevant quantities, suggests that complete self-preservation could be plausible. If such a scaling exists, it would rely on a more sophisticated transformation than the one arising from a single set of similarity variables. Notably, such a scaling should account for the relative behaviour of the different similarity variables. Section IV D addresses this issue.

D. Log-similarity of energy spectra and structure functions

The main idea is to use both outer and inner variables in a single representation for energy spectra and structure functions. In other words, instead of invoking only **one** set of velocity, length, and scalar characteristic scales, a new type of normalization could be proposed using **two** sets

of similarity variables: one targeting the large-scales, the other the small-scales. Then one should define an appropriate transformation so that the relative behaviour between outer and inner scales is accounted for. One solution is a log-type similarity. This type of similarity solution is not new. It has been first observed and justified for the temperature field in a Rayleigh-Bénard convection flow²⁸ and further investigated in detail for the dynamical field in fully developed homogeneous isotropic turbulence.^{29–31}

Let us first define two functions $f_\delta^{u_\alpha}$ and $f_{\eta_K}^{u_\alpha}$ such as

$$f_\delta^{u_\alpha} = \frac{\log\left(C_1 \frac{(\overline{\Delta u_\alpha})^2}{U_0^2}\right)}{\log\left(\frac{U_0^2}{u_K^2}\right)}, \quad (21a)$$

$$f_{\eta_K}^{u_\alpha} = \frac{\log\left(C_1 \frac{(\overline{\Delta u_\alpha})^2}{u_K^2}\right)}{\log\left(\frac{U_0^2}{u_K^2}\right)}. \quad (21b)$$

Here $f_\delta^{u_\alpha}$ and $f_{\eta_K}^{u_\alpha}$ ($u_\alpha \equiv u, v$) are, respectively, functions of r_δ and r_{η_K} defined by

$$r_\delta = \frac{\log\left(C_2 \frac{r}{\delta}\right)}{\log\left(\frac{\delta}{\eta_K}\right)}, \quad (22a)$$

$$r_{\eta_K} = \frac{\log\left(C_2 \frac{r}{\eta_K}\right)}{\log\left(\frac{\delta}{\eta_K}\right)}. \quad (22b)$$

C_1 and C_2 are two constants. For the scalar field, similar definitions can be proposed

$$f_\delta^\theta = \frac{\log\left(C_1 \frac{(\overline{\Delta \theta})^2}{\Delta \theta_0^2}\right)}{\log\left(\frac{\Delta \theta_0^2}{\theta_B^2}\right)}, \quad (23a)$$

$$f_{\eta_B}^\theta = \frac{\log\left(C_1 \frac{(\overline{\Delta \theta})^2}{\theta_B^2}\right)}{\log\left(\frac{\Delta \theta_0^2}{\theta_B^2}\right)}, \quad (23b)$$

$$r_\delta = \frac{\log\left(C_2 \frac{r}{\delta}\right)}{\log\left(\frac{\delta}{\eta_B}\right)}, \quad (23c)$$

$$r_{\eta_B} = \frac{\log\left(C_2 \frac{r}{\eta_B}\right)}{\log\left(\frac{\delta}{\eta_B}\right)}. \quad (23d)$$

From Eqs. (21a), (21b), (22a), and (22b), it can be shown that

$$f_\delta^{u_\alpha}(r_\delta) = f_{\eta_K}^{u_\alpha}(r_{\eta_K} - 1) - 1. \quad (24)$$

This very general identity holds for any set of similarity variables (as far as they are different) and is not limited only to (δ, U_0) and (η_K, u_K) . Equation (24) suggests that if $f_\delta^{u_\alpha}(r_\delta)$ is self-similar, then so does $f_{\eta_K}^{u_\alpha}(r_{\eta_K})$ since they are related by a simple translation. Therefore, this has the major advantage of circumventing the particular choice of similarity variables that can be made for normalization and hence, a universal scaling independent of the sets of similarity variables is likely to emerge. Similar definitions can be proposed for the energy spectra

$$E_\delta^{u_\alpha} = \frac{\log\left(C_1 \frac{4\pi^2 E_{u_\alpha}}{U_0^2 \delta}\right)}{\log\left(\frac{U_0^2 \delta}{u_K^2 \eta_K}\right)}, \quad (25a)$$

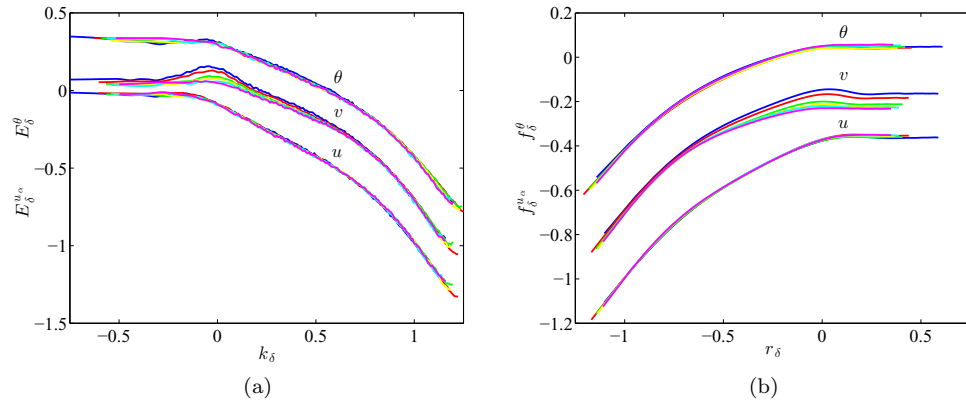


FIG. 7. Log-similarity for the energy spectra and structure functions. (a) Energy spectra with $C_1 = 0.25$ and $C_2 = 1$, spectra of v and θ are shifted upwards by factors of 0.2 and 0.4, respectively. (b) structure functions with $C_1 = 0.25$ and $C_2 = 1$, structure functions of v and θ are shifted upwards by factors of 0.2 and 0.4, respectively.

$$E_{\eta_K}^{u_\alpha} = \frac{\log\left(C_1 \frac{4\pi^2 E_{u_\alpha}}{u_K^2 \eta_K}\right)}{\log\left(\frac{U_0^2 \delta}{u_K^2 \eta_K}\right)}, \quad (25b)$$

$$E_\delta^\theta = \frac{\log\left(C_1 \frac{4\pi^2 E_\theta}{\Delta\theta_0^2 \delta}\right)}{\log\left(\frac{\Delta\theta_0^2 \delta}{u_B^2 \eta_B}\right)}, \quad (25c)$$

$$E_{\eta_B}^\theta = \frac{\log\left(C_1 \frac{4\pi^2 E_\theta}{\theta_B^2 \eta_B}\right)}{\log\left(\frac{\Delta\theta_0^2 \delta}{u_B^2 \eta_B}\right)}, \quad (25d)$$

which are, respectively, functions of k_δ and $k_{\eta_{K,B}}$,

$$k_\delta = \frac{\log(2\pi C_2 k \delta)}{\log\left(\frac{\delta}{\eta_{K,B}}\right)}, \quad (26a)$$

$$k_{\eta_{K,B}} = \frac{\log(2\pi C_2 k \eta_{K,B})}{\log\left(\frac{\delta}{\eta_{K,B}}\right)}. \quad (26b)$$

Similarly, it is straightforward to show that

$$E_\delta^{u_\alpha}(k_\delta) = E_{\eta_K}^{u_\alpha}(k_{\eta_K} - 1) - 1. \quad (27)$$

The prefactor 2π in Eqs. (26a) and (26b) and the factor $4\pi^2$ in Eqs. (25a) and (25b) arise from the definition of the wavenumber and the Fourier Transform, respectively. It is interesting to note that this log-similarity law is quite similar to the one proposed by Refs. 30 and 31. Indeed, using, e.g., Eqs. (19c) and (19c), the expression for the energy spectra can be recast as follows:

$$E_\delta^{u_\alpha} \propto \frac{\log\left(\frac{E_{u_\alpha}}{E^\dagger}\right)}{\log\left(\frac{R_\delta}{R^\dagger}\right)}, \quad (28a)$$

$$k_\delta \propto \frac{\log\left(\frac{k}{k^\dagger}\right)}{\log\left(\frac{R_\delta}{R^\dagger}\right)}, \quad (28b)$$

where E^\dagger , R^\dagger , and k^\dagger are some constants which are introduced here only for convenience. The log-similarity as given here by Eqs. (21a), (21b), (25a), and (25b) thus appears to be analogous to the log-similarity law proposed by Refs. 29–31.

The log-similarity has been tested using the present measurements and the results are presented in Figs. 7(a) and 7(b). With the exception of v for which, as already mentioned, the coherent motion contributes significantly to the energy distribution at large scales, the log-similarity law seems to be satisfied closely over the whole range of scales. Pragmatically speaking, this type of scaling acts as a compression-dilatation transformation of the spectra (or structure functions) and wavenumbers (or separations) so that they all fall onto a single curve. As a consequence, the analytical considerations of Refs. 30 and 31 on the basis of a multifractal analysis, are likely to apply here to theoretically justify the plausibility of a log-similarity in the axisymmetric mixing layer, albeit the quite low Reynolds number of the flow. The values for C_1 and C_2 were empirically assessed and set to 0.25 and 1, respectively. Further investigations are needed to provide a physical interpretation for these constants and to explore their dependence on the initial conditions, the Reynolds number and the type of flow.

V. CONCLUSION

Self-preservation for one- and two-point statistics in the slightly heated axisymmetric mixing layer of a round jet has been investigated by means of hot- and cold-wire anemometry. Special care has been paid to the reliability of the present measurements for which use was made of (i) a 60° X wire probe, calibrated by a look-up table method, to capture high velocity angles and high turbulence levels, (ii) a local convection velocity in Taylor's hypothesis, and (iii) an instantaneous correction method for the cold-wire time response.

Analysis of one-point statistics reveals that the dynamical and scalar fields follow different approaches towards self-similarity, the latter being reached more rapidly for u than for v and θ . Altogether, all these quantities appear to attain a self-preserving state at $x = 3.5D$ corresponding to a Reynolds number Re_δ based on the upstream velocity U_0 and the shear layer momentum thickness δ of 6.4×10^3 . It is clear that the approach to similarity of v'/U_0 and \overline{uv}/U_0^2 is delayed relative to that for u'/U_0 . This is interpreted as being caused by the footprint of coherent structures whose contribution is mostly perceptible on v and progressively decreases as x increases. Spectra and structure functions of v corroborate this interpretation.

Four different sets of similarity variables are tested for normalizing spectra and structure functions. For this purpose, in addition to the scales L_S^u and U_S which pertain to the dynamical field, a shear length-scale L_S^θ and characteristic temperature scale θ_S are introduced on the basis of the scale-by-scale budget for the second-order temperature structure function. L_S^u and L_S^θ allow the range of scales which is affected by the presence of the mean velocity and temperature gradient, to be assessed. They are believed to be relevant quantities for a slightly heated mixing layer. Experimental data reveal that the shear variables behave as outer variables, i.e., L_S^u and L_S^θ are proportional to δ , while U_S and θ_S scale as U_0 and θ_0 , respectively. This is simply explained by the self-similar behaviour of the normalized mean energy and scalar dissipation rates.

Since the Reynolds number R_λ increases significantly with the streamwise distance x , complete self-preservation is not attainable. Instead, the range of scales complying with self-similarity depends on the particular choice of similarity variables. A similarity analysis of the two-point transport equation featuring only the production term has been performed and confirms this. Komogorov variables appear to be suitable at small and intermediate scales, i.e., in the range $\eta_{K,B} \leq r \lesssim L_S^{u,\theta}$. George's similarity variables are adequate for normalizing the very small- and very large-scales but there are significant departures at intermediate scales where the nonlinear energy transfer dominates. We noted also a bias, in the context of George's similarity, associated with the non-negligible contribution of coherent motion to the velocity variance. On the other hand, outer and shear variables lead to a satisfactory collapse of spectra and structure functions at large and intermediate scales down to the cross-over length-scale between viscous and inertial effects.

Log-similarity, which accounts for the variations of R_λ or equivalently the relative behaviour between outer and inner variables, has been introduced and tested. Instead of using a single set of length, velocity, or temperature characteristic scales for normalizing two-point statistics, log-similarity relies on two sets of similarity variables. This has the major advantage of circumventing the particular choice of the two sets of similarity variables since it was proven that, e.g., $f_\delta(r_\delta)$

and $f_{\eta_K}(r_{\eta_K})$ are related by a simple translation transformation. Results show that log-similarity applies for all scales with a very high degree of accuracy. This observation opens the door to new perspectives for using the log-similarity hypothesis in flows where R_λ varies such as grid turbulence in the initial period, the far field of a plane jet or the intermediate wake region. However, while at very high Reynolds numbers, the inertial range is sufficiently developed for log-similarity to be an intuitive or plausible scaling, at low to moderate Reynolds numbers, there should be a limit in terms of variations of R_λ for the log-similarity to be satisfied. Indeed, variations in curvature of second-order structure functions (or spectra) in the pseudo-inertial range, which result from variations of R_λ , are unlikely to be compensated indefinitely by a simple compression-dilatation transformation. The plausibility of the log-similarity in turbulence should further be demonstrated on a dynamical basis (i.e., the scale-by-scale budget) rather than on phenomenological arguments using multifractal models. These issues are left for future work. The two constants C_1 and C_2 were introduced and assessed empirically. Further work is also needed to investigate in detail their physical meaning and their dependence on the Reynolds number, initial conditions, or the type of flow.

ACKNOWLEDGMENTS

L.D. and R.A.A. are grateful to the Australian Research Council for its support.

- ¹R. W. Stewart and A. A. Townsend, "Similarity and self-preservation in isotropic turbulence," *Philos. Trans. Roy. Soc. London* **243**, 359–386 (1951).
- ²W. K. George, "The decay of homogeneous isotropic turbulence," *Phys. Fluids* **4**, 1492–1509 (1992).
- ³C. G. Speziale and P. S. Bernard, "The energy decay in self-preserving isotropic turbulence revisited," *J. Fluid Mech.* **241**, 645–667 (1992).
- ⁴R. A. Antonia, R. J. Smalley, T. Zhou, F. Anselmet, and L. Danaila, "Similarity of energy structure functions in decaying homogeneous isotropic turbulence," *J. Fluid Mech.* **487**, 245–269 (2003).
- ⁵W. K. George, "Self-preservation of temperature fluctuations in isotropic turbulence," in *Studies in Turbulence* (Springer, 1992), pp. 514–528.
- ⁶J. R. Chasnov, "Similarity states of passive scalar transport in isotropic turbulence," *Phys. Fluids* **6**, 1036–1051 (1994).
- ⁷M. Gonzalez and A. Fall, "The approach to self-preservation of scalar fluctuations decay in isotropic turbulence," *Phys. Fluids* **10**, 654–661 (1998).
- ⁸R. A. Antonia and P. Orlandi, "Similarity of decaying isotropic turbulence with a passive scalar," *J. Fluid Mech.* **505**, 123–151 (2004).
- ⁹R. A. Antonia, R. J. Smalley, T. Zhou, F. Anselmet, and L. Danaila, "Similarity solution of temperature structure functions in decaying homogeneous isotropic turbulence," *Phys. Rev. E* **69**, 016305-1–016305-11 (2004).
- ¹⁰W. K. George and M. M. Gibson, "The self-preservation of homogeneous shear flow turbulence," *Exp. Fluids* **13**, 229–238 (1992).
- ¹¹L. Danaila, F. Anselmet, and T. Zhou, "Turbulent energy scale-budget equations for nearly homogeneous sheared turbulence," *Flow, Turbul. Combust.* **72**, 287–310 (2004).
- ¹²P. M. Bevilacqua and P. S. Lykoudis, "Turbulence memory in self-preserving wakes," *J. Fluid Mech.* **89**, 589–606 (1978).
- ¹³W. K. George, "The self-preservation of turbulent flows and its relation to initial conditions and coherent structures," in *Advances in Turbulence*, edited by W. K. George and R. Arndt (Springer, Berlin, 1989), pp. 39–74.
- ¹⁴R. D. Moser, R. M. Moser, and D. W. Ewing, "Self-similarity of time-evolving plane wakes," *J. Fluid Mech.* **367**, 255–289 (1998).
- ¹⁵R. A. Antonia and J. Mi, "Approach towards self-preservation of turbulent cylinder and screen wakes," *Exp. Therm. Fluid. Sci.* **17**, 277–284 (1998).
- ¹⁶D. Ewing, W. K. George, M. M. Rogers, and R. D. Moser, "Two-point similarity in temporally evolving plane wakes," *J. Fluid Mech.* **577**, 287–307 (2007).
- ¹⁷F. Thiesset, R. A. Antonia, and L. Danaila, "Scale-by-scale turbulent energy budget in the intermediate wake of two-dimensional generators," *Phys. Fluids* **25**, 115105 (2013).
- ¹⁸L. J. S. Bradbury, "The structure of a self-preserving turbulent plane jet," *J. Fluid Mech.* **23**, 31–64 (1965).
- ¹⁹R. A. Antonia, B. R. Satyaprakash, and A. K. M. F. Hussain, "Measurements of dissipation rate and some other characteristics of turbulent plane and circular jets," *Phys. Fluids* **23**, 695–700 (1980).
- ²⁰D. Ewing, B. Frohnappfel, W. K. George, J. Pedersen, and J. Westerweel, "Two-point similarity in the round jet," *J. Fluid Mech.* **577**, 309–330 (2007).
- ²¹P. Burattini, R. A. Antonia, and L. Danaila, "Similarity in the far field of a turbulent round jet," *Phys. Fluids* **17**, 025101 (2005).
- ²²F. Thiesset, R. A. Antonia, and L. Djenidi, "Consequences of self-preservation on the axis of a turbulent round jet," *J. Fluid Mech.* **748**, R2 (2014).
- ²³P. Bradshaw, "The effect of initial conditions on the development of a free shear layer," *J. Fluid Mech.* **26**, 225–236 (1966).
- ²⁴G. L. Brown and A. Roshko, "On density effects and large structure in turbulent mixing layers," *J. Fluid Mech.* **64**, 775–816 (1974).

- ²⁵ H. E. Fiedler, "On turbulence structure and mixing mechanism in free turbulent shear flows," in *Turbulent Mixing in Nonreactive and Reactive Flows* (Springer, 1975), pp. 381–409.
- ²⁶ A. K. M. F. Hussain and M. F. Zedan, "Effects of the initial condition on the axisymmetric free shear layer: Effects of the initial momentum thickness," *Phys. Fluids* **21**, 1100–1112 (1978).
- ²⁷ A. K. M. F. Hussain and M. F. Zedan, "Effects of the initial condition on the axisymmetric free shear layer: Effect of the initial fluctuation level," *Phys. Fluids* **21**, 1475–1481 (1978).
- ²⁸ X.-Z. Wu, L. Kadanoff, A. Libchaber, and M. Sano, "Frequency power spectrum of temperature fluctuations in free convection," *Phys. Rev. Lett.* **64**, 2140–2143 (1990).
- ²⁹ M. Nelkin, "Multifractal scaling of velocity derivatives in turbulence," *Phys. Rev. A* **42**, 7226 (1990).
- ³⁰ U. Frisch and M. Vergassola, "A prediction of the multifractal model: The intermediate dissipation range," in *New Approaches and Concepts in Turbulence* (Springer, 1993), pp. 29–34.
- ³¹ B. Castaing, Y. Gagne, and M. Marchand, "Log-similarity for turbulent flows?" *Physica D* **68**, 387–400 (1993).
- ³² I. Wygnanski and H. E. Fiedler, "The two-dimensional mixing region," *J. Fluid Mech.* **41**, 327–361 (1970).
- ³³ F. H. Champagne, Y. H. Pao, and I. J. Wygnanski, "On the two-dimensional mixing region," *J. Fluid Mech.* **74**, 209–250 (1976).
- ³⁴ P. Burattini, R. A. Antonia, S. Rajagopalan, and M. Stephens, "Effect of initial conditions on the near-field development of a round jet," *Exp. Fluids* **37**, 56–64 (2004).
- ³⁵ A. K. M. F. Hussain and A. R. Clark, "On the coherent structure of the axisymmetric mixing layer: A flow-visualization study," *J. Fluid Mech.* **104**, 263–294 (1981).
- ³⁶ H. H. Bruun, *Hot Wire Anemometry: Principles and Signal Analysis* (Oxford University Press, 1995).
- ³⁷ W. W. Willmarth and T. J. Bogar, "Survey and new measurements of turbulent structure near the wall," *Phys. Fluids* **20**, S9–S21 (1977).
- ³⁸ R. M. Lueptow, K. S. Breuer, and J. H. Haritonidis, "Computer-aided calibration of x-probes using a look-up table," *Exp. Fluids* **6**, 115–118 (1988).
- ³⁹ P. Burattini and R. A. Antonia, "The effect of different x-wire schemes on some turbulence statistics," *Exp. Fluids* **38**, 80–89 (2005).
- ⁴⁰ J. Lemay and A. Benaïssa, "Improvement of cold-wire response for measurement of temperature dissipation," *Exp. Fluids* **31**, 347–356 (2001).
- ⁴¹ H. E. Fiedler, "On data acquisition in heated turbulent flows," in *Proceedings of the Dynamic Flow Conference 1978 on Dynamic Measurements in Unsteady Flows* (Springer, 1978), pp. 81–100.
- ⁴² R. A. Antonia, L. W. B. Browne, and A. J. Chambers, "Determination of time constants of cold wires," *Rev. Sci. Instrum.* **52**, 1382–1385 (1981).
- ⁴³ K. Bremhorst and L. J. W. Graham, "A fully compensated hot/cold wire anemometer system for unsteady flow velocity and temperature measurements," *Meas. Sci. Technol.* **1**, 425–430 (1990).
- ⁴⁴ G. Xu and R. A. Antonia, "Effect of different initial conditions on a turbulent round free jet," *Exp. Fluids* **33**, 677–683 (2002).
- ⁴⁵ S. D. Rajagopalan and R. A. Antonia, "Properties of the large structure in a slightly heated turbulent mixing layer of a plane jet," *J. Fluid Mech.* **105**, 261–281 (1981).
- ⁴⁶ A. Kolmogorov, "The local structure of turbulence in incompressible viscous fluid for very large Reynolds numbers," *Proc. R. Soc. London A* **434**(1890), 9–13 (1991).
- ⁴⁷ C. M. Casciola, P. Gualtieri, R. Benzi, and R. Piva, "Scale-by-scale budget and similarity laws for shear turbulence," *J. Fluid Mech.* **476**, 105–114 (2003).
- ⁴⁸ S. Corrsin, "Local isotropy in turbulent shear flow," Tech. Rep., NACA RM, 1958.
- ⁴⁹ L. Danaïla and L. Mydlarski, "Effect of gradient production on scalar fluctuations in decaying grid turbulence," *Phys. Rev. E* **64**, 016316 (2001).
- ⁵⁰ A. A. Townsend *The structure of turbulent shear flows*, edited by G. Batchelor (Cambridge University Press, 1956).
- ⁵¹ P. A. Davidson and B. R. Pearson, "Identifying turbulent energy distributions in real, rather than fourier, space," *Phys. Rev. Lett.* **95**, 214501 (2005).
- ⁵² H. Mouri and A. Hori, "Two-point velocity average of turbulence: Statistics and their implications," *Phys. Fluids* **22**, 115110 (2010).
- ⁵³ A. Attili and F. Bisetti, "Statistics and scaling of turbulence in a spatially developing mixing layer at $Re_\lambda = 250$," *Phys. Fluids* **24**, 035109 (2012).
- ⁵⁴ A. Attili and F. Bisetti, "Fluctuations of a passive scalar in a turbulent mixing layer," *Phys. Rev. E* **88**, 033013 (2013).
- ⁵⁵ F. Thiesset, L. Danaïla, and R. A. Antonia, "Dynamical effect of the total strain induced by the coherent motion on local isotropy in a wake," *J. Fluid Mech.* **720**, 393–423 (2013).
- ⁵⁶ F. Thiesset, L. Danaïla, and R. Antonia, "Dynamical interactions between the coherent motion and small scales in a cylinder wake," *J. Fluid Mech.* **749**, 201–226 (2014).